Int. J. Electrochem. Sci., 12 **(2017)** 4392 – 4405, doi: 10.20964/2017.05.58

International Journal of ELECTROCHEMICAL SCIENCE
www.electrochemsci.org

Electrocatalytic Hydrogen Production Properties of Poly(3-aminobenzoic acid) doped with Metal Organic Frameworks

Kabelo E. Ramohlola[1], Milua Masikini[2], Siyabonga B. Mdluli[2], Gobeng R. Monama[1], Mpitloane J. Hato[1], Kerileng M. Molapo[2], Emmanuel I. Iwuoha[2], Kwena D. Modibane[1,]*

[1] Department of Chemistry, School of Physical and Mineral Science, University of Limpopo, Polokwane, Sovenga 0727 South Africa
[2] SensorLab, Chemistry Department, University of the Western Cape, Cape Town, South Africa
[*]E-mail: kwena.modibane@ul.ac.za

Received: 30 November 2016 / *Accepted:* 14 February 2017 / *Published:* 12 April 2017

The design and development of inexpensive highly efficient electrocatalysts based on polymer organometallic composites for hydrogen production, underpins several emerging clean-energy technologies. In this work, for the first time, Poly(3-aminobenzoic acid) based metal organic framework (PABA/MOF) composite was synthesized by chemical oxidation of 3-aminobenzoic acid monomer in the presence of metal organic framework (MOF) content. Poly(3-amino benzoic acid) (PABA), MOF and PABA/MOF composite were characterized by ultraviolet visible (UV-vis) and fourier transform infrared (FTIR) spectroscopy, powder X-ray diffraction (XRD), thermal gravimetric analysis (TGA), scanning electron microscope (SEM), transmission electron microscope (TEM), energy dispersive X-ray spectroscopy (EDS, EDX), selected area electron diffraction (SAED) and cyclic voltammetry (CV). Detailed structural and morphological characterizations established that PABA is wrapping MOF. Furthermore, spectroscopic analyses provided information that MOF was incorporated on the backbone of PABA as indicative of an easier path for the electron transport and plentiful active sites for the catalysis of hydrogen evolution reaction (HER) in acidic electrolyte. Experiments probing the electrochemical properties revealed that the composite was very stable and robust and had exceptionally properties. Significant HER was generated by the composite in dimethyl sulfoxide/*tetrabutylammonium perchlorate (*DMSO/TBAP) supporting electrolyte in the presence of hydrogen source by applying a potential to the electrode.

Keywords: poly(3-aminobenzoic acid), metal organic frameworks, electrochemistry, hydrogen evolution reaction, Tafel plot.

1. INTRODUCTION

Intrinsic conducting polymers (ICPs) such as polyacetylene (PA), polypyrrole (PPyP, polythiopene (PTh) polyaniline (PANI) and poly(p-phenylenevinylene) (PVP) have shown good

conductive, optoelectrical and luminescence properties and have been applied in most electrochemical applications [1]. Among all ICPs, PANI has been widely studied for electronic and optical applications due to its exceptional conducting, optical and mechanical properties [1,2]. However, there is a limitation to the application of polyaniline due to its non-processibility which results from poor solubility in most organic solvents such as dimethylsulfoxide (DMSO), dimethylformamide (DMF) and N-methyl-2-pyrrolidone (NMP) [3, 4]. One of the methods towards tackle the non-processibility of polyaniline, is to synthesize new aniline polymers from aniline monomer derivatives [5]. Sulfonated polyaniline has been used in many studies with little attention paid on polyaniline with parent carboxylic acid group [6-8]. Amino benzoic acid (ABA), which differs with the positions (meta- (m), ortho- (o) and para- (p) of the carboxylic acid (COOH) and amine group (NH_2) is one of aniline derivatives which is capable of forming conducting polymer containing electron-rich nitrogen atom and high electron density of carbonyl group [7,8]. The amine and carboxylic group are easily polymerized and polymerization can occur using the same radical mechanism as unsubstituted polyaniline.

Furthermore, the carboxylic acid group which is not altered during polymerization reaction serves as a functional group that can be used as a matrix material to immobilize other substrates or form covalent bonds with other materials such as nanomaterials [9]. Recently, an increased interest in applying polyaniline and its derivatives to fuel and photoelectrochemical cells has been observed [10,11]. In fuel cells, it is expected that electrocatalyst materials exhibit the capability of sustaining high current densities with low overpotentials [12,13]. In particular, polyaniline has proved to be capable of activating the hydrogen evolution reaction (HER). In the current study, 3-aminobenzoic acid was selected as the starting monomer of the polymerization for comparing the activities of these polymers as electrocatalyst. Carboxyl groups can be used to combine with the metal on MOF surface by a multi-bridging chelating coordination. MOF materials are constructed by joining metal-containing units (secondary building units (SBUs)) with organic linkers, using strong bonds (reticular synthesis) which gives the material the unique chemical properties such open crystalline frameworks with permanent porosity [14,15]. The synthesized PABA/MOF obtained by oxidative chemical polymerization of amino benzoic acid monomer in the presence of MOF were characterized by FTIR, UV-visible spectra, SEM, TEM, EDS, EDX, TGA and SAED. The current study also aims to show the efforts in understanding the electrocatalysis mechanism of the HER over PABA, MOF and PABA/MOF composites. It is necessary to point that, to date, no evidence has been presented in the scientific literature for the polymerization of 3-amino benzoic acid in the presence of MOF for hydrogen evolution reaction.

2. EXPERIMENTAL SECTION

2.1. Materials

3-aminobenzoic acid monomer (ABA), copper nitrate trihydrate ($Cu(NO_3).3H_2O$), trimesic acid (H_3BTC) and tetrabutylammonium percholate (TBAP) were purchased from Sigma Aldrich, South

Africa. Ammonium per sulfate (APS) and iron chloride ($FeCl_3$) were purchased from Riedel-de Haen and Educhem, respectively. Absolute ethanol was purchased at Merck, South Africa. Hydrochloric acid (HCl), dimethyl sulfoxide (DMSO) and sulphuric acid (H_2SO_4) were procured from Rochelle Chemicals. H_2SO_4 standard solutions were made in DMSO solution with 0.1 M TBAP as a supporting electrolyte system unless otherwise stated. All measurements were carried out at 22±2°C.

2.2. Methods

2.2.1. Preparation of PABA, MOF and PABA/MOF composite

Poly(3-aminobenzoic acid)(PABA) was prepared by oxidation polymerization of 3-amino benzoic acid (ABA) monomer according to a previously reported method [16]. The synthesis of Cu-trimesic MOF (HKUST-1) was based on a previously reported hydrothermal procedure [15] The synthesis of PABA doped with metal organic framework composite referred as PABA/MOF. Approximately, 1 g of the 3-aminobenzoic monomer and 3.6 wt.% MOF were dissolved in a solution of 10 ml HCl/100 ml distilled water in a 250 ml round-bottom flask. The solution was stirred for 30 minutes at 50 ^{O}C where after 2.40 g of ammonium persulfate (APS), $(NH_4)_2S_2O_8$, and 1.88 g of $FeCl_3$ were added respectively in the solution. The resulting mixture was stirred for another 3 hours at 50 ^{O}C and the content of the reaction was placed in the oven at 50 ^{O}C overnight to evaporate the solvents and remaining content was washed with ethanol and dried at 50 ^{O}C.

2.2.2. Characterization Techniques

Absorbance spectra were recorded on a Varian Cary 300 UV-Vis-NIR spectrophotometer using 1 cm optical path length quartz cuvette. Morphological characterizations were performed using Auriga Field Emission Scanning Electron Microscope (FESEM) coupled with EDS detector for elemental analysis and transmission electron micrographs were collected using an FEI Tecnai G2 20 field-emission gun (FEG) TEM, operated in bright field mode at an accelerating voltage of 200 kV. Energy dispersive x-ray spectra were collected using an EDAX liquid nitrogen cooled Lithium doped Silicon detector. The crystal structure of the PABA/MOF nanocomposite was analyzed by using SAED and Phillips PW 1830 model XRD. The FTIR spectra were acquired on a Cary 600 series FTIR spectrometer (Agilent Technologies). The samples for FTIR measurement were prepared by grinding the dried sample powder mixed with potassium bromide (KBr) to a fine powder and then compressing under high pressure into thin pellets. Electrochemical measurements were performed using EPSILON electrochemical workstation performed in 10 ml of 0.1 M DMSO/TBAP electrolytic system. Prior to scans, the working electrode was cleaned by successive polishing using 1, 0.3 and 0.05 μm alumina micro polish and polishing pads purchased from Buehler, IL, USA, followed by rinsing with deionized water and sonication in ethanol and water to remove all traces of alumina polish. After sonication, the electrodes were rinsed with ethanol and deionized water and dried under a nitrogen stream. The data was collected using a conventional three-electrode set-up with gold electrode (3 mm diameter) as a working electrode, platinum wire as a counter electrode and Ag/AgCl wire as a reference electrode.

Repetitive scanning of the solutions of the complexes MOF, PABA and PABA/MOF (~10 mg) was from -0.20 to 1.20 V at scan rates of 0.02-0.10 Vs^{-1}. Experimental measurements for HER studies have been carried out at different concentration of H_2SO_4 as hydrogen source in DMSO/TBAP system.

3. RESULTS AND DISCUSSION

3.1. Synthesis

Scheme 1 shows the synthesis of PABA/MOF composite from the mixed solutions of 3-aminobenzoic acid and ammonium peroxodisulfate in the presence of MOF. The 3-aminobenzoic acid has an aromatic structure similar to aniline that can be polymerized to polyaniline by an oxidation reaction [17] and grow on the surface of MOF. In the reaction, $(NH_4)_2S_2O_8$ is used as an oxidizing agent in a strongly acidic environment for the reaction. It was reported that introduction of $(NH_4)_2S_2O_8$ solution into the aminobenzoic acid solution, free radicals as initiating agent produced by breaking peroxodisulfate can attract the activated hydrogen of amino group of aminobenzoic acid, resulted new free radical of aminobenzoic acid molecular [17,18].

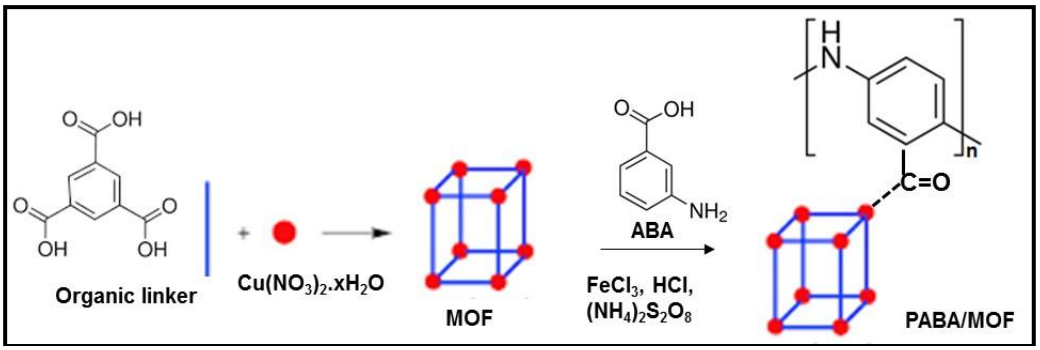

Scheme 1. Synthesis of poly(aminobenzoic acid) based MOF composites through oxidation polymerization of aminobenzoic monomer in the presence of MOF material.

The new free radical can attract with aminobenzoic acid molecular, and then reacts with the initiating agent to complete a substitution reaction on the aromatic ring by free radicals. This substitution product can be attracted and lengthened further by free radical of aminobenzoic acid molecular [17]. The product of high molecular weight can be precipitated from reacting solution. Therefore, polymerizations of lengthened chain can be ended, and formed PABA with carboxyl groups attached onto MOF surface as shown in Scheme 1.

3.2. Spectroscopic characterizations

FTIR spectrum of synthesized composite with reference to PABA and MOF spectra is shown in Figure 1(a). It can be seen that the aminobenzoic acid has a sharp ν(N–H) bands located at around

3500~3300 cm^{-1} [19,20] which was changed to broad bands after the polymerization reaction. The band at 1745 cm^{-1} is assigned to the ν(C=O) group of carboxylic acid [17] in both composite and PABA. The peak at 1588 cm^{-1} is attributed to COO^- asymmetric stretch and medium band at 1438 cm^{-1} due to $–COO^-$symmetric stretch of the carboxylate group. The FTIR spectra also show vibration bands at 545 and 1256 cm^{-1} which are attributed to C-C and in-plane C-H bonding modes, respectively. Two bands at 761 and 838 cm^{-1} are due to out-of phase C-H [21,22].

The UV-visible absorption spectra of synthesized composite and PABA in DMSO solvent are shown in Figure 1(b). It is observed that all samples reveal a broad absorption band between 300 and 600 nm which can be attributed to the π-π^* transition of the benzenoid rings and the exciton transition of the quinoid rings, respectively, for polymer and composite [19,23]. The slightly bathochromic shift was observed for the composite compared with PABA due to the presence of MOF through carboxylate attachment, increase electron density of the polymer backbone. These observations were also demonstrated before when PABA incorporate with nanocomposite or materials [24].

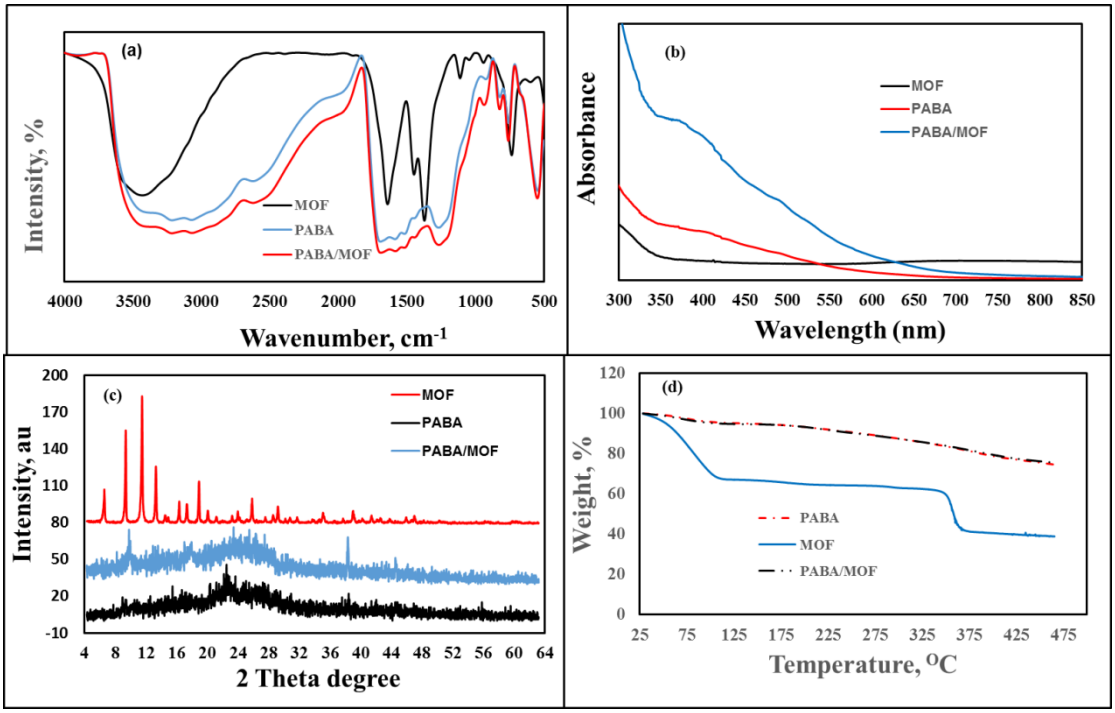

Figure 1. (a) FTIR, (b) UV-vis spectra of PABA, MOF and PABA/MOF in DMSO, (c) XRD and TGA analysis of MOF, PABA and PABA/MOF.

The XRD patterns of PABA, MOF and PABA/MOF composite are shown in Figure 1(c). The MOF pattern show that the MOF phases are highly crystalline, which is an indication of micro-porous materials characteristics [25]. The XRD pattern of PABA shows a broad peak at 2θ angle of 25^o which indicates that synthesis of PABA was successful and it is also in accordance to the previous reported data on the XRD result of polyaniline [21]. In situ addition of MOF during polymerization process resulted in decrease in the XRD intensities of PABA with appearance of new sharp peak at 2θ angle of 10^o which is an indicative that MOF is doped in PABA backbone to form a composite.

The thermal stability of the PABA, MOF, and PABA/MOF samples was investigated using TGA, as shown in Figure 1(d). The decomposition temperature of the TGA curves indicates that MOF decomposes in two weight loss steps whereas PABA and its composite showed to be thermally stable. For MOF, the initial weight loss took place at 50– 100 ^{O}C is due to the loss of water bound molecules or moisture. The weight loss for MOF at temperatures around 350 ^{O}C indicates a structural decomposition of the MOF framework.

3.3. Morphological characterizations

Figure 2 shows the SEM images of (a) MOF, (c) PABA and (e) PABA/MOF and EDS elemental composition of (b) MOF, (d) PABA and (f) PABA/MOF samples. The SEM morphological images of MOF and PABA show a typically octahedral-shaped with smooth surfaces (Figure 2(a)) and hollow ball-like (Figure 2(c)), respectively.

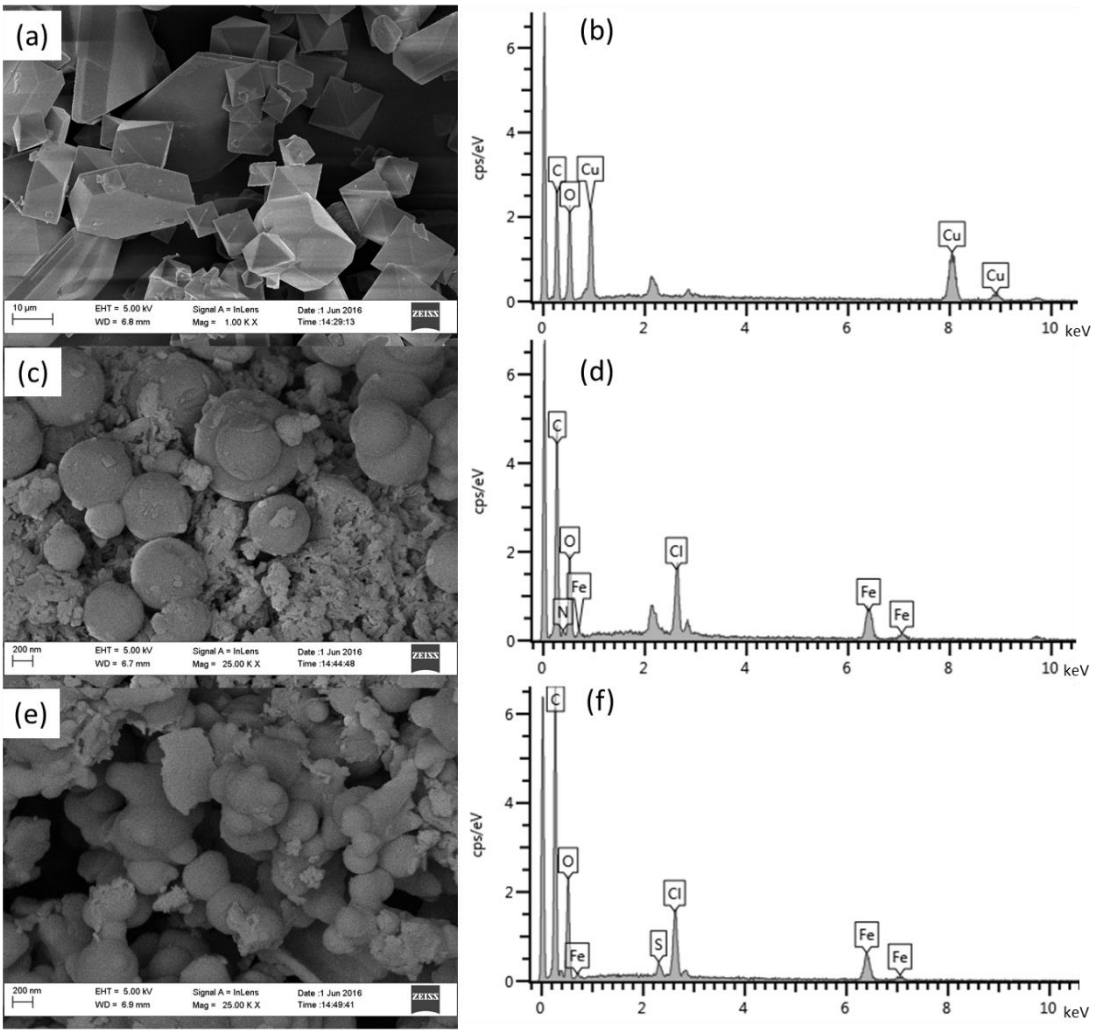

Figure 2. SEM image of (a) MOF, (c) PABA, (e) PABA/MOF composite and EDS spectrum of (b) MOF, (d) PABA, (f) PABA/MOF composite.

It is observed in Figure 2(e) that the morphology shows grain-like with introduction MOF on the polymer backbone as compared to spherical, granular and hollow ball-like for PABA (Figure 2(c)) [6, 19, 26-28]. The elemental composition of PABA/MOF composite from EDS (Figure 2(f)) showed an increase in the percentage compositions of C and O and there was no Cu metal of MOF detected on the surface of polymer as compared to the EDS of MOF (Figure 2(d)). From the SEM and EDS analysis, it can be deduced that PABA is wrapping around the MOF bundles as noncovalent attachment between PABA and MOF.

The TEM and SAED (inset) images for MOF, and PABA are shown in Figure 3(a) and (b) respectively. The MOF images show that the MOF phases are highly crystalline, which is an indication of micro-porous materials characteristics. The TEM image of PABA is in accordance to the previous reported data on the morphology of poly(3-aminobenzoic acid) [6]. The SAED inset image of PABA reveals a clear diffraction ring and spot of the polycrystalline characteristics. The PABA wrapping around MOF as an observed in SEM above (Figure 2(e) was further confirmed by TEM image (Figure 3(c)) showing the presence of MOF covered by polymer. The elemental analysis on TEM image using EDX (Figure 3(b)) showed an increased in carbon and oxygen content in the composite as compared to PABA. The copper content of MOF was detected however it overlapped with the foreign species of the grid.

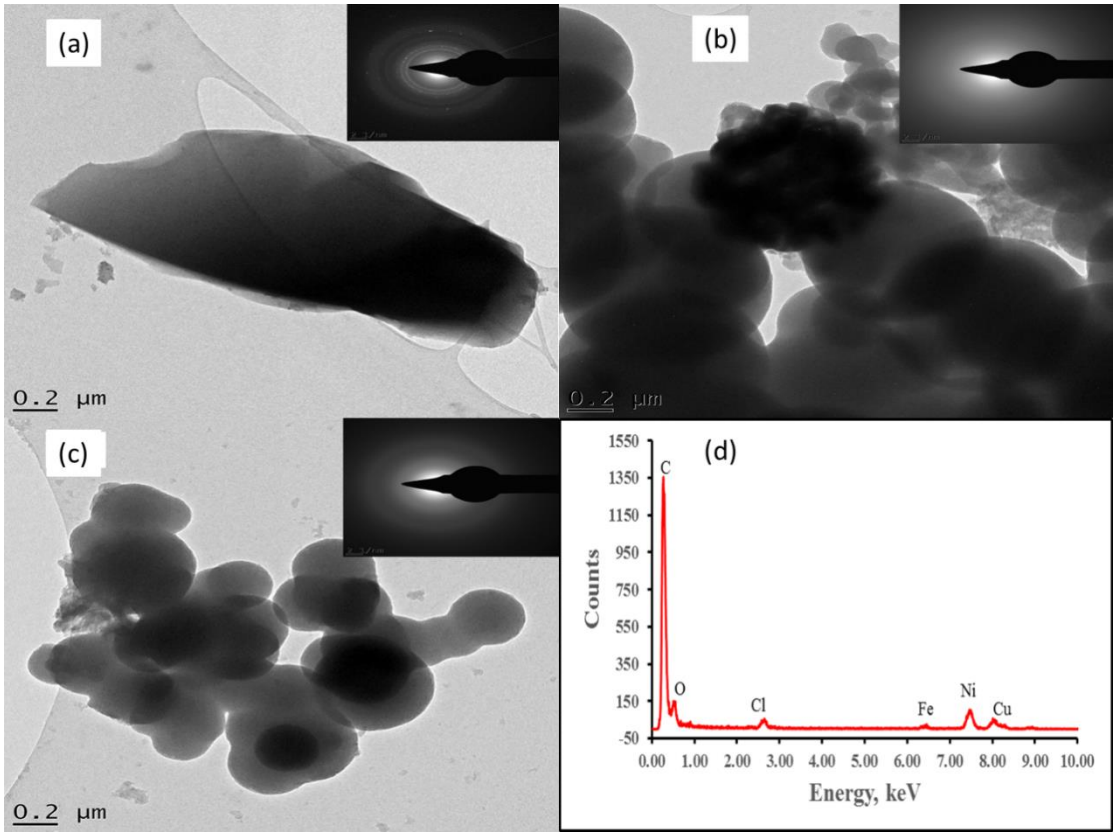

Figure 3. TEM images (a) MOF, (b) PABA, (c) PABA/MOF composite and (d) EDX spectrum of PABA/MOF composite. Inset: SAED image.

The inset image in Figure 3(c) is SAED for structural identification and it showed that the composite maintains its amorphous structure of PABA (Figure 3(b)). However, it has spot where the d-spacing of the composite can be determined as indicative of modification of structural properties of the polymer with MOF and supported by the XRD (Figure 1(c)).

3.4. Electrochemical characterizations

Cyclic voltammetry characterizations of PABA and PABA/MOF were achieved by using a gold (Au) electrode in a 0.1 M TBAP/DMSO electrolyte at a scan rate of 0.1V/s and are recorded in Figure 4(a). The electrochemical properties of the materials was monitored by two ways;1) change in current density at oxidation-reduction potential in relation to bare Au electrode and 2) appearance of new oxidation or/and reduction peaks or respective anodic or cathodic peaks. The voltammogram of a bare Au electrode showed a typical redox couple at E_{pc} ~ -0.6 and E_{pa} ~ -0.8V which is due to migration of ion from the electrolyte solution to the Au electrode in order to maintain system equilibrium [29]. The voltammogram in the presence of PABA showed increase in current density as compared to the bare electrode.

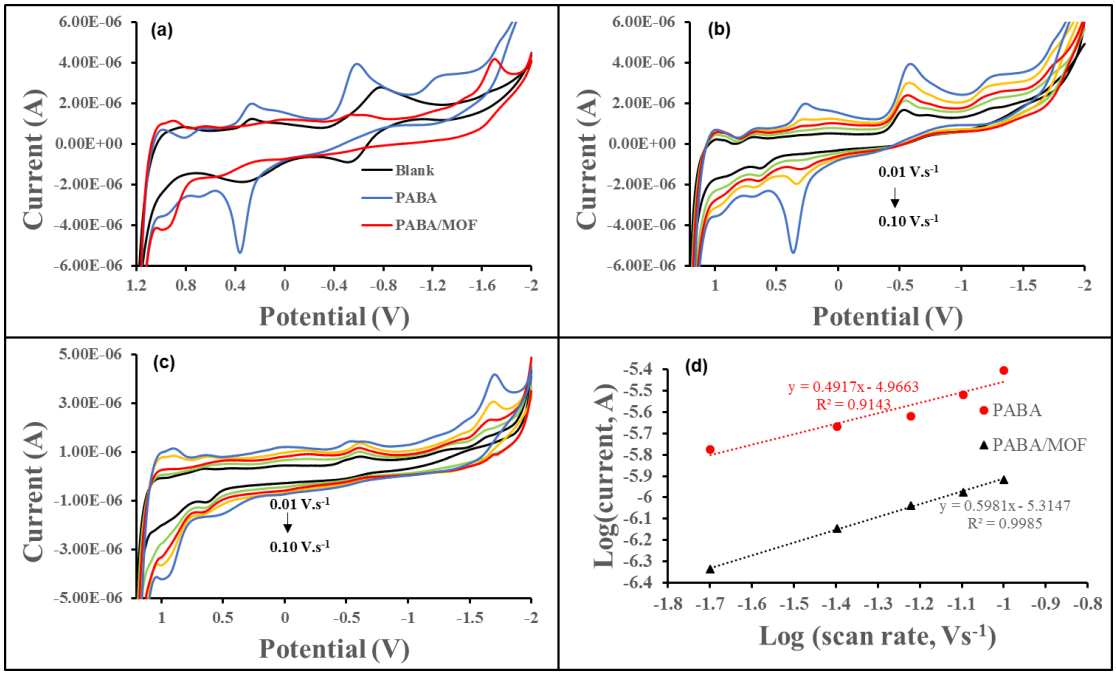

Figure 4. (a) CV results of PABA and PABA/MOF at 0.1 Vs^{-1}; (b) and (c) CV of PABA and PABA/MOF at different scan rates (0.02- 0.10 Vs^{-1}); and (d) The log-log plot of the absolute value of the peak current vs scan rate for the PABA and PABA/MOF materials at 0.02 to 0.1 Vs^{-1} in 0.1 M DMSO/TBAP electrolyte solution on gold electrode.

However, the presence of carboxylic group on the polymer backbone of PABA makes the voltammogram of PABA to be different from the one of pure polyaniline (PANI), thus the three redox peaks which can be attributed to different oxidation state of PANI will not be observed [30]. When MOF is introduced, there is a collapse of the oxidation and reduction peaks on the same region and an

increase in cathodic peak intensity at lower potential which agree with the requirement of electrocatalyst [13]. The decrease in current density of the composite materials shows that during composite formation, the conductivity of PABA material was affected by incorporation of MOF.

The different scan rate dependent studies were used to examine the dynamic electrochemical properties of (b) PABA and (c) PABA/MOF during oxidation-reduction processes and are shown in Figure 4. The figures show that the current density of the materials increased with the increase scan rate and cathodic peak current shifting towards negative potential with increasing scan rate as indicative of quasi-reversible process [31]. The increase in peak current with increase scan rates shows that there is an electric charge-transfer controlled process in all materials. Figure 4(d) shows the plot of the logarithm of the absolute value of the reductive peak current against the logarithm of the scan rate. The result shows a linear relationship with a slope of 0.492 and 0.598 for PABA and PABA/MOF materials, respectively. These slope values are close to the expected value of 0.5 as indicative of semi-finite diffusion control [32]. The 0.5 slope shows that the peak current is directly proportional to the square root of the scan rate [32]. The diffusion controlled process was also supported by current proportionality to square root of scan rate in the range of 0.02- 0.10 V/s for quasi-reversible couple as demonstrated in Figure 5.

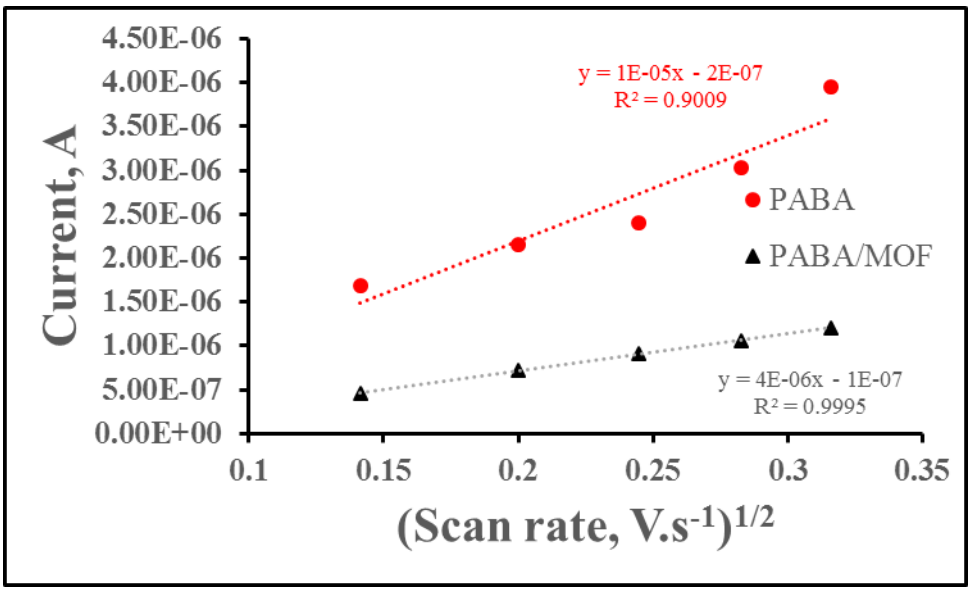

Figure 5. Peak current as a function of square root of scan rate on gold in 0.1 M DMSO/TBAP electrode system at different scan rates (0.02 – 0.10 Vs^{-1}).

To accurately determine kinetic rate constants and other parameters, the diffusion coefficient, *D*, was determined for catalysts using cyclic voltammetry and following the Randles-Ševćik equation (Eq. 1) for a quasi-reversible system [31]:

$$Ip = (2.65 \times 10^5)n^{3/2}ACD^{1/2}v^{1/2} \quad [1]$$

n is the number of electrons transferred, *A* is the electrode area in cm^2, *D* is the diffusion coefficient in $cm^2\ s^{-1}$, *C* is the bulk molar concentration of the electroactive species in $mol.cm^{-3}$ and *v*

is scan rate is Vs^{-1}. The diffusion coefficient was determined to be 5.2 x 10^{-7} and 0.83 x 10^{-7} cm^2 s^{-1} for PABA and PABA/MOF composite, respectively. The value indicates that the movement of electrons along the polymer chain was averagely fast and agrees well with diffusion coefficient values reported for doped polyaniline [33].

3.5. Hydrogen evolution reaction

Upon addition of sulphuric acid, two reduction peaks appeared within the potential window of DMSO (Figure 6(a)). An irreversible wave appeared between -0.40 and -0.90 V. This reductive wave is followed immediately by a large cathodic current that is assigned to the catalytic reduction of protons to dihydrogen. Notably, reductive wave had no corresponding oxidative wave on the positive potential sweep. For the catalytic wave at -1.80 V, it represents the evolution of hydrogen gas, an irreversible process. This irreversibility was attributed to the reduction being coupled to the complex accepting two protons from solution [34].

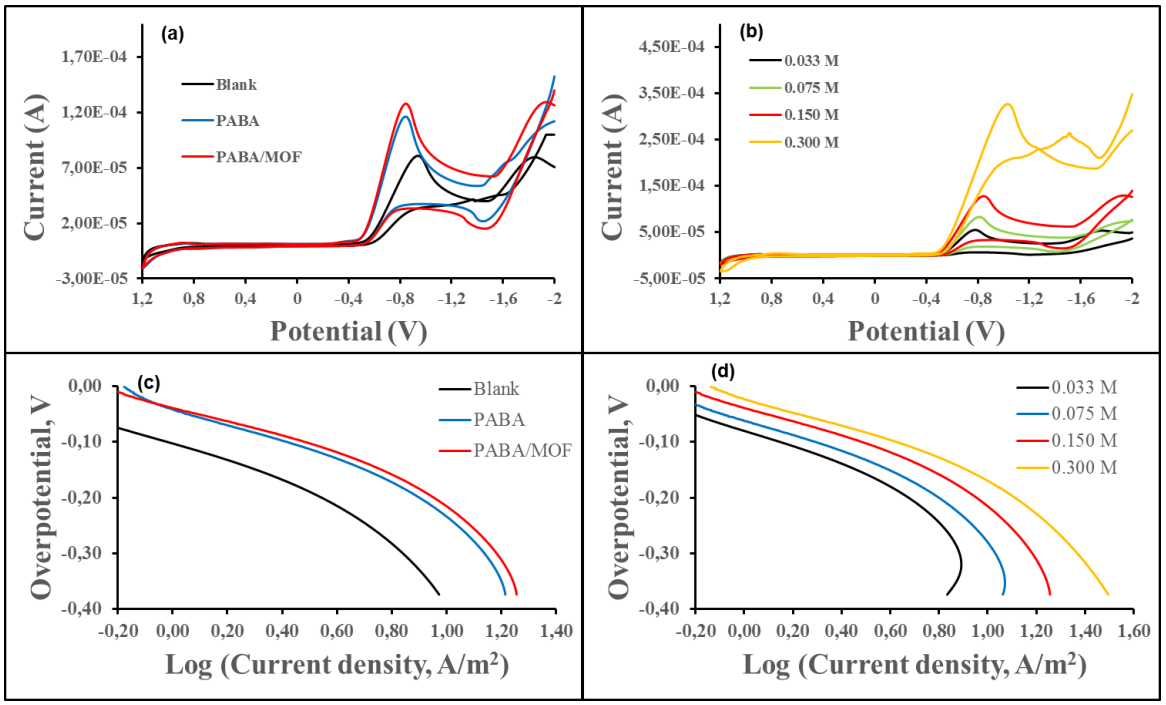

Figure 5. (a) CV and (c) Tafel plots of PABA and PABA/MOF in the presence 0.15 M H_2SO_4; (b) CV and (d) Tafel plots of PABA/MOF at 0.10 Vs^{-1} in the presence of different H_2SO_4 concentration on gold electrode in 0.1 M DMSO/TBAP electrode system.

To determine the overpotential required to evolve hydrogen at the catalyst, a cyclic voltammogram was taken of a solution of sulphuric acid in DMSO using a gold electrode. The onset of cathodic current at gold in DMSO is -0.460 V in the presence of sulphuric acid (Figure 6(a), curve blank) as the control experiment to assure the catalyst was responsible for the currents observed. There

was a small background current representing thermodynamically favourable, but kinetically hindered reduction of protons at the working electrode [35].

This is a good determination for the thermodynamic potential required for the hydrogen evolution reaction to proceed, as gold is known to evolve hydrogen from acidic solutions with minimal overpotential [36]. Using this value, it was estimated that the catalysts evolved hydrogen with an overpotential of approximately -0.405 V. In 0.15 M solution of sulphuric acid, the current at around -0.882 V was ~2 times less in the absence of PABA and PABA/MOF, than with it present.

To ascertain that proton reduction was the source of the catalytic current, cyclic voltammograms of catalyst were performed in the presence of increasing concentrations of sulphuric acid. Figure 6(b), there was reductive current observed in the presence of PABA/MOF using a gold (Au) electrode in a 0.1 M DMSO/TBAP electrolyte at a scan rate of 0.10 Vs^{-1} for different acid concentrations. This supports that both reductive waves in the voltammogram above needed protons to proceed.

Tafel plots were recorded to determine the kinetic parameters in the absence and presence of PABA, and PABA/MOF that allow the evaluation of both exchange current density *i*o and cathodic transfer coefficient 1-*α*. Creţu *et al*.; [36] and Khanova and Krishtalik [37] have proved that on gold in sulphuric acid solution, Tafel plots present two distinct slopes at low and high overpotential corresponding to the HER controlled by desorption of the hydrogen atoms and charge transfer mechanism as a slow step of the cathodic process, respectively. Therefore, in order to determine kinetic parameters that characterize the charge transfer, Tafel slopes were plotted for a limiting domain of high overpotentials and presented in Figure 6(c) and (d). The transfer coefficient 1–*α* was calculated using high overpotential region, where the Butler–Volmer equation simplifies to the Tafel equation, from the Tafel slope *b* given by relationship:

$$b = \frac{-2.303\,RT}{(1-\alpha)F} \quad [2]$$

where *R* is the gas constant (8.31451 J mol^{-1} K^{-1}), *T* - thermodynamic temperature (K), *F* – Faraday's number (96,485 C mol^{-1}). The exchange currents *i*o were evaluated from Tafel slope intersection with the abscissa (log(I_0)).

It was reported that the Tafel slope*b* is an important parameter as it can reveal the mechanisms of the HER in aqueous acid solutions which proceed in a series of three elementary reaction which comprises of two electrochemical steps and one chemical steps [38, 39]. The three elementary reaction steps (Eq. 3-5) in acidic medium are:

$H^+ + e^- \rightarrow H_{ad}$ Volmer reaction [3]

$H_{ad} + H^+ + e^- \rightarrow H_2$ Heyrovsky reaction [4]

$H_{ad} + H_{ad} \rightarrow H_2$ Tafel reaction [5]

The combination of steps (3 and 4) or (3 and 5) can lead to the production of molecular H_2. Kinetic models of the HER, under a specific set of conditions have shown that a slope of ~120 mV/dec is indication of Volmer step, while a rate determining Heyrovsky or Tafel step should produce slopes between 30-40 $mV.dec^{-1}$. These values can be used as a guide in identifying HER mechanisms. The measured values slopes for the materials are listed in Table 1. Gold electrode exhibits the slope of

106.2 and 167.4 mV.dec^{-1} at 0.300 and 0.150 M H_2SO_4 concentrations, respectively which is used as a control. Upon addition of PABA and PABA/MOF, at 0.300 M H_2SO_4, there is an increase in slope as compared to the Au electrode. This is in accordance with the reported results by Zheng *et. al*. [40] and Corte *et. al.* [41]. The similar behaviour was observed in polyaniline nickel electrode (Ni-PANI, Table 1) with a slope of 147 mV.dec^{-1} in 0.5 M H_2SO_4 [41]. At low concentration, the slope decreased with respect to Au electrode towards the Volmer slope, 120 mV.dec^{-1}. This shows that there is an adsorption of hydrogen proton on the surface of the materials and number of adsorption sites increases once the composites is formed since there is a further decrease in slope. According to the data presented in Table 1, it can be observed that in the absence and presence of PABA and PABA/MOF composite, the charge transfer coefficient 1–α decreases with decrease in concentration of H_2SO_4. To explain this phenomenon it is necessary to take into account that the charge transfer coefficient 1–α represents a measure of the activated complex coordinates at the metal – electrolyte solution interface [40, 41]. The lower the value of 1–α, the further is the reaction plane from the metal surface which was the case with the PABA/MOF composite. The low value of 1–α was documented to be 0.33 (or α=0.67) for Cu-Pt bimetallic nanoparticles supported metal organic framework-derived nanoporous carbon Cu-Pt-NPCC [42]. The resulting current densities (i_0) from Tafel plots, confirmed the benefits of MOF incorporation on polymer for the HER (Table 1). The current density obtained for composite at 0.300 M H2SO4 was ca. 2 and times higher than the current density observed on the control electrode. These current densities were also higher than the one Ni-PANI and Cu-Pt-NPCC (Table 1) reported before.

Table 1. Experimental values of Tafel slope, transfer coefficient 1–α and exchange current *i*o, in the absence and presence of PABA and PABA/MOF composite.

Material	H_2SO_4 [mol/L]	Slope (b) [V.dec^{-1}]	-b [mV.dec^{-1}]	1-α	logi_0	i_0 [A.m^2]
Blank	0.300	-0.1062	106.2	0.57	1.25	17.78
	0.150	-0.1674	167.4	0.35	0.98	09.55
PABA	0.300	-0.1237	123.7	0.48	1.45	28.18
	0.150	-0.1535	153.5	0.39	1.30	19.95
PABA/MOF	0.300	-0.1305	130.5	0.45	1.55	35.48
	0.150	-0.1355	135.5	0.44	1.35	22.39
	0.075	-0.1469	146.9	0.40	1.22	16.60
	0.033	-0.1602	160.2	0.37	1.10	12.60
Ni-PANI [41]	0.500	-0.1470	147.0	[a]	0.17	01.47
Cu-Pt-NPCC [42]	0.500	[a]	[a]	0.33	-2.62	0.002

a= no reported literature value

4. CONCLUSIONS

We demonstrate the preparation of novel poly(3-aminobenzoic acid)/metal organic framework composite through in situ polymerization of 3-aminobenzoic acid (aniline derivative) in the presence of MOF. Structural and morphological characterizations showed that incorporation was successful

with PABA polymer wrapping MOF. The catalytic effect of PABA and PABA/MOF composites on HER was studied using exchange current density and charge transfer coefficient determined by the Tafel slope method. A drastic increase in catalytic H_2 evolution was observed in PABA and composite. Moreover, they merely require overpotentials as low as ~-0.405 V to attain current densities of ~0.8 and 1.5 Am^{-2} and show good long-term stability. All these characteristics meet requirements for HER electrocatalysts for hydrogen fuel cell. The improved catalytic activity observed in this work can be attributed to the following factors (i) increase in electron density of the polymer by introduction of MOF, which allows efficient electron transfer between the electron rich edges and the electrode and (ii) presence of Cu atom, which plays a crucial role in catalyzing the electrochemical HER (iii) improvement of photophysical and electrochemical properties of the PABA and PABA/MOF composite, which substantially improves the charge transfer kinetics of HER. We have demonstrated that the HER performance of PABA and PABA/MOF composite varies significantly with incorporation of MOF. The polymerization method reported here for PABA/MOF material is scalable and can be extended to obtain other MOF based catalysts with different MOF loading and therefore represents an important development toward HER and other energy conversion technologies.

ACKNOWLEDGEMENT
The authors would like to thank the financial supports from the National Research Foundation (NRF) of South Africa under the Unique Grant No. 99278 and University of Limpopo (Grants: R202 and R232).

References

1. S. Bhadra, D. Khastgir,N.K. Singha and J.H. Lee, *Prog. Polym. Sci.*, 34 (2009) 783.
2. J. Stejskal, I. Sapurina, M. Trchova, *Prog. Polym. Sci.*, 35 (2010) 1420.
3. S. Bilal, S. Gul, R. Holze and A.H.A. Shah, *Synth. Met., 206* (2015) 131.
4. A. Abdolahi, E. Hamzah, Z. Ibrahim, S. Hashim, *Materials., 5* (2012) 1487.
5. K. Kamaraj, V. Karpakam, S. Sathiyanarayanan and G. Ventakachari, *Mater. Chem. Phys., 122* (2010) 123.
6. I.A. Sophia, G. Gopu and C. Vedhi, *Open J. Synt. Theo. Appl., 1* (2012) 1.
7. R.S.D. Sangeetha, P.T. Arasu, G.H. Kumar and R.S.D. Bella, *Int. J. ChemTech Res., 6* (2014) 5335.
8. C. Thiemann and C.M.A. Brett, *Synth. Met., 123* (2001) 1.
9. P. Netsuwan, W. Chaisu, S. Phanichphant and S. Sriwichai, *Adv. Mater. Sci. Eng., 2014* (2014) Article ID 873028, 6 pages, http://dx.doi.org/10.1155/2014/873028
10. Z. Chen, L. Xu, W. Li, M. Waje and Y. Yan, *Nanotechnology., 17* (2006) 5254-5259.
11. J. Liu, S. Lu, X. Liang, Q. Gan, Y. Wang and H. Li, *J. Electroanal. Chem., 764* (2016) 15.
12. M. Zeng and Y. Li. *J. Mater. Chem. A., 3* (2015) 14942.
13. A. Vargas-Uscategui, E. Mosquera, B. Chornik and L. Cifuentes, *Electrochim. Acta., 178* (2015) 739.
14. H. Hosseini, H. Ahmar, A. Dehghani, A. Bagheri, A. Tadjarodi and A.R. Fakhari, *Biosens. Bioelectron*., 42 (2003) 426.
15. F. Ke, L.G. Qiu, Y.P. Yuan, F.M. Peng, X. Jiang, A.J. Xie, Y.H. Shen and J.F. Zhu, *J. Hazar. Mater., 196* (2011) 36.
16. T. David, J.K. Mathad, T. Padmavathi and A. Vanaja, *Polymer., 55* (2014) 5665.

17. S. Patra and N. Munichandraiah, *Synt. Met.*, 150 (2005) 285.
18. P. Wen and X. Wang, *J. Nanomater.*, (2013) doi:10.1155/2013/795652.
19. E.N. Zare, M.M. Lakouraj and E. Moosavi, *Composite interfaces.*, (2016) doi: 10.1080/09276440.2016.1156966.
20. M. Sharifirad, F. Kiani and F. Koohyar, *Eur. Online J. Nat. Soc. Sci., 2* (2013) 366.
21. A. Mostafaei and A. Zolriasatein, *Prog. Nat. Scie: Mater. Int.*, 22 (2012) 273.
22. A. Benyoucef, F. Huerta, J.L. Va´zquez and E. Morallon, *Eur. Polym. J., 41* (2005) 843.
23. M.P. Dash, M. Tripathy, A. Sasmal, G.C. Mohanty and P.L. Nayak, *J. Mater. Sci., 45* (2010) 3858.
24. R. Golshaei, Z. Guler, C. Ünsal and A.S. Sarac, *Eur. Polym. J., 66* (2015) 502.
25. K.S. Lin, A.K. Adhikari, C.N. Ku, C.L. Chiang and H. Kou, *Int. J. Hydrogen Energy., 37* (2012) 13865.
26. E. Mildan and M. Gulfen, *J. Appl. Polym. Sci., 132* (2015) 42533.
27. S. Ranganathan, P. Raju, V. Arunachalam, G. Krishnamoorty, M. Ramadoss, S. Arumainathan and N. Vengidusamy, *Bull. Korean Chem Soc., 33* (2012) 1919.
28. A.K. Singh, L. Joshi, R. Prakash and K. Kaneto, *Jpn. J. Appl. Phys., 49* (2010) 1.
29. M.M. Rahman and I.C. Jeon, *J. Braz. Chem. Soc., 18* (2007) 1150.
30. D. Giray, T. Balkan, B. Dietzel and A.S. Sarac. *Eur. Polym. J., 49* (2013) 2645.
31. J. Yang and S. Gunasekaran, *Carbon., 51* (2013) 36.
32. R. Tucceri, *TOPCJ., 4* (2010) 62.
33. E.I. Iwuoha, D.S. De-Villaverde and M.R. Smyth, *Biosens. Bioelectron., 12* (1997) 753.
34. P.S. Guin, S. Das and P.C. Mandal, *Int. J. Electrochem.*, (2011) doi:10.4061/2011/816202.
35. A.B.P. Lever, *J. Porphyrins Phthalocyanines., 3* (1999) 488.
36. R. Cretu, A. Kellenberger, M. Medeleanu and N. Vaszilcsin, *Int. J. Hydrogen Energy., 9* (2014) 4465.
37. A.K. Khanova and L.I. Krishtalik, *J. Electroanal. Chem., 660* (2011) 224.
38. B.E. Conway, *Sci. Prog., 71* (1987) 479.
39. Y. Zheng, Y. Jiao, M. Jaroniec and S.Z. Qiao, *Ange. Chem. Int. Ed., 54* (2015) 52.
40. Z. Zheng, N. Li, C.Q. Wang, D.Y. Li, Y.M. Zhu and G. Wu, *Int. J. Hydrogen Energy., 37* (2012) 13921.
41. D.A.D. Corte, C. Torres, P. S. Correa, E.S. Rieder and C.F. Malfatti, *Int. J. Hydrogen Energy., 37* (2012) 3025.
42. S. Mandegarzad, J.B. Raoof, S. R. Hosseini and R. Ojani, *Electrochim. Acta., 190* (2016) 729.